PB87-113429

Off-Center Spherical Model for Dosimetry Calculations in Chick Brain Tissue

(U.S.) Health Effects Research Lab.
Research Triangle Park, NC

1986

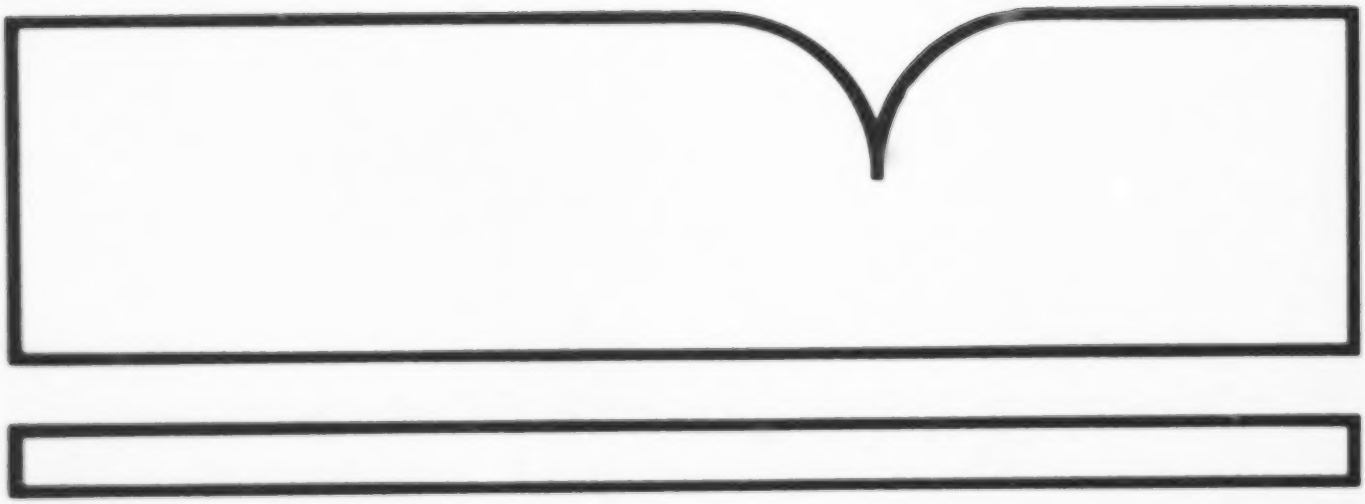

U.S. Department of Commerce
National Technical Information Service
NTIS

TECHNICAL REPORT DATA

(Please read Instructions on the reverse before complet

1. REPORT NO.	2.	3.
EPA/600/J-86/170		PB87-113429

4. TITLE AND SUBTITLE
Off-Center Spherical Model for Dosimetry Calculations in Chick Brain Tissue (Journal Version)

5. REPORT DATE
1986

6. PERFORMING ORGANIZATION CODE

7. AUTHOR(S)
*Guillermo Gonzalez,*James C. Nearing,+Ronald J. Spiegel and+William T. Joines

8. PERFORMING ORGANIZATION REPORT NO.

9. PERFORMING ORGANIZATION NAME AND ADDRESS
*University of Miami
+HERL, EBD, BEB

10. PROGRAM ELEMENT NO.

11. CONTRACT/GRANT NO.
68-02-4092

12. SPONSORING AGENCY NAME AND ADDRESS
Health Effects Research Laboratory - RTP, NC
Office of Research and Development
U.S. Environmental Protection Agency
Research Triangle Park, NC 27711

13. TYPE OF REPORT AND PERIOD COVERED

14. SPONSORING AGENCY CODE
EPA/600/11

15. SUPPLEMENTARY NOTES
This paper is not the final report under contract #68-02-4092
REF: Bioelectromagnetics. 7:209-221, April 1986

16. ABSTRACT

This paper presents calculations for the electric field and absorbed power density distribution in chick brain tissue inside a test tube, using an off-center spherical model. It is shown that the off-center spherical model overcomes many of the limitations of the concentric spherical model, and permits a more realistic modeling of the brain tissue as it sits in the bottom of the test tube surrounded by buffer solution. The effect of the unequal amount of buffer solution above the upper and below the lower surfaces of the brain is analyzed. The field distribution is obtained in terms of a rapidly converging series of zonal harmonics. A method that permits the expansion of spherical harmonics about an off-center origin in terms of spherical harmonics at the origin is developed to calculate in closed form the electric field distribution. Numerical results are presented for the absorbed power density distribution at a carrier frequency of 147 MHz. It is shown that the absorbed power density increases toward the bottom of the brain surface. Scaling relations are developed by keeping the electric field intensity in the brain tissue the same at two different frequencies. Scaling relations inside, as well as outside, the brain surface are given. The scaling relation distribution is calculated as a function of position, and compared to the scaling relations obtained in the concentric spherical model. It is shown that the off-center spherical model yields scaling ratios in the brain tissue that lie between the extreme values predicted by the concentric and isolated spherical models.

17. KEY WORDS AND DOCUMENT ANALYSIS

a. DESCRIPTORS	b. IDENTIFIERS/OPEN ENDED TERMS	c. COSATI Field/Group

18. DISTRIBUTION STATEMENT	19. SECURITY CLASS (This Report)	21. NO. OF PAGES
RELEASE TO PUBLIC	UNCLASSIFIED	15
	20. SECURITY CLASS (This page)	22. PRICE
	UNCLASSIFIED	

EPA/600/J-86/170
JOURNAL ARTICLE

Bioelectromagnetics 7:209–221 (1986)

Off-Center Spherical Model for Dosimetry Calculations in Chick Brain Tissue

Guillermo Gonzalez, James C. Nearing, Ronald J. Spiegel, and William T. Joines

Departments of Electrical and Computer Engineering (G.G.) and Physics (J.C.N.), University of Miami, Coral Gables, Florida; and Experimental Biology Division, U.S. Environmental Protection Agency, Research Triangle Park, North Carolina (R.J.S., W.T.J.)

This paper presents calculations for the electric field and absorbed power density distribution in chick brain tissue inside a test tube, using an off-center spherical model. It is shown that the off-center spherical model overcomes many of the limitations of the concentric spherical model, and permits a more realistic modeling of the brain tissue as it sits in the bottom of the test tube surrounded by buffer solution. The effect of the unequal amount of buffer solution above the upper and below the lower surfaces of the brain is analyzed. The field distribution is obtained in terms of a rapidly converging series of zonal harmonics. A method that permits the expansion of spherical harmonics about an off-center origin in terms of spherical harmonics at the origin is developed to calculate in closed form the electric field distribution. Numerical results are presented for the absorbed power density distribution at a carrier frequency of 147 MHz. It is shown that the absorbed power density increases toward the bottom of the brain surface. Scaling relations are developed by keeping the electric field intensity in the brain tissue the same at two different frequencies. Scaling relations inside, as well as outside, the brain surface are given. The scaling relation distribution is calculated as a function of position, and compared to the scaling relations obtained in the concentric spherical model. It is shown that the off-center spherical model yields scaling ratios in the brain tissue that lie between the extreme values predicted by the concentric and isolated spherical models.

Key words: brain tissue, radiofrequency, radiation, dosimetry, calcium ions

INTRODUCTION

A problem of considerable importance to the understanding of biological phenomena produced by electromagnetic radiation is the mechanism of interaction of amplitude-modulated radiofrequency (RF) waves on calcium-ion efflux from in vitro chick brain [Bawin et al, 1975; Blackman et al, 1979, 1980a, 1980b, 1981, 1985; Sheppard et al, 1979]. These works have demonstrated that RF radiation, when amplitude modulated with extremely low frequency (ELF) sinusoidal waves, can enhance the calcium-ion efflux from in vitro chick brain tissue.

Received for review April 29, 1985; revision received November 20, 1985.

This paper has been reviewed by the Health Effects Research Laboratory, U.S. Environmental Protection Agency (EPA), and approved for publication. Mention of trade names or commercial products does not constitute endorsement or recommendation for use. The opinions expressed in this paper are those of the authors and do not necessarily reflect official EPA opinion.

Address reprint requests to Guillermo Gonzalez, Department of Electrical and Computer Engineering, University of Miami, Coral Gables, FL 33124.

© 1986 Alan R. Liss, Inc.

NTIS is authorized to reproduce and sell this report. Permission for further reproduction must be obtained from the copyright owner.

The calcium-ion efflux phenomenon has several interesting aspects. It occurs only when the RF carrier wave is amplitude modulated at ELF. The peak effect occurs with 16 Hz amplitude-modulated RF fields, and no effect has yet been observed with unmodulated RF carrier waves, or with modulation frequencies below 6 Hz or above 50 Hz. The calcium-ion efflux occurs at only certain electric field intensities in the chick brain. Biological experiments [Joines and Blackman, 1980] have shown that the effect also occurs at other carrier frequencies if the average electric field intensity in the chick brain remains the same. That is, the effect also occurs if the incident power density is adjusted by an amount that compensates for the change in frequency and complex permittivity of the chick brain.

In order to understand the effects of amplitude-modulated RF radiation on calcium-ion efflux better, the electromagnetic fields and absorbed power density distribution in the chick brain must be accurately determined. Concentric spherical models [Joines and Blackman, 1980, 1981; Joines et al, 1981] have been developed to calculate the field and absorbed power density distribution in the chick brain. These models have provided much valuable information about the dosimetric aspects of the calcium-ion efflux experiments. The models have also been used to determine the required incident power density that produces calcium-ion efflux at other carrier frequencies.

Internal electric field strengths [Weil et al, 1984] have been measured inside chick forebrains exposed under the same conditions as those used by Blackman et al [1979, 1980a, 1980b]. This experimental study found that the measured ratio between 50 and 147 Mhz was in reasonable agreement with values predicted by the concentric spherical model. Because of the relative large size of the electric field probe (6% of the half-brain volume), only the field strength at the center of the brain could be measured. Therefore, the field distribution inside the brain, as well as surface electric fields, could not be determined by the use of this probe.

This study overcomes the limitations of the concentric spherical models and also some inherent restrictions of the experimental methods. Concentric spherical models do not adequately represent the chick brain immersed in the buffer medium, because the brain, as it sits in the bottom of the test tube, is surrounded by a layer of buffer solution with a thickness that is different above and below the brain. Concentric spherical models use a uniform layer of buffer solution to surround the brain. To determine the dosimetric effects of the nonuniform layer, an off-center spherical model is used to approximate the physical geometry of the brain/buffer combination. The off-center spherical model represents a significant refinement to the concentric spherical model because the brain can be modeled as a continuous, smooth, spherical surface surrounded by unequal amounts of buffer solution on its upper and lower surfaces. The electric field and absorbed power density distributions, and scaling ratios for carrier waves of 50, 100, and 147 MHz are calculated using a quasi-static approximation. This approximation leads to a field representation in terms of a convergent series involving spherical harmonics.

THEORETICAL DEVELOPMENT

The schematic of the experimental set up is shown in Figure 1. The chick brain tissue sits at the bottom of the test tube and it is surrounded by a nonuniform layer of buffer solution. The hemispherical bottom of the test tube has an inner radius of 0.71

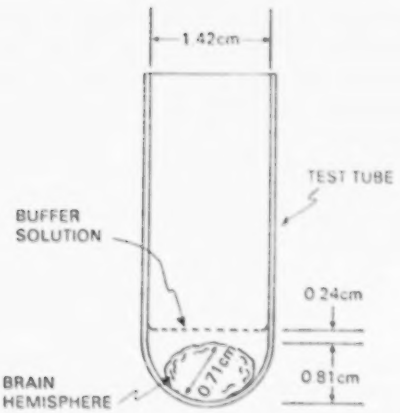

Fig. 1. Schematic of the chick brain inside a test tube containing a buffer solution.

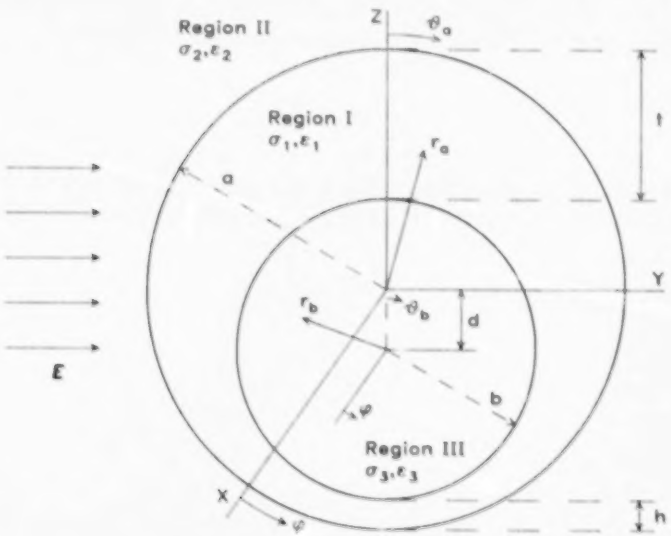

Fig. 2. Off-center spherical model for the chick brain.

cm. The chick brain has a mean horizontal dimension of 1 cm and a mean height of 0.81 cm. The mean height from the top of the tissue to the surface of the buffer solution is 0.24 cm.

The analytical model for the off-center spherical model of the brain inside a test tube is shown in Figure 2, along with the direction of the incident electric field. This model represents the geometry in Figure 1. In fact, except for the flat-topped buffer region the model is reasonably accurate. The radii a and b, and the off-center distance d are selected so that the brain volume occupies 0.3 ml, and the buffer volume 1 ml. Also, the limiting case as h approaches zero is analyzed.

The mathematical formulation that follows is by no means a simple extension of the concentric spherical case. To the best of our knowledge exact solutions to off-center spherical geometries, of the type shown in Figure 2, in terms of zonal harmonic expansions have not appeared in the literature. However, a simpler problem involving an off-center spherical capacitor is given in Morse and Feshbach [1953: pp 1270–1273], together with an ingenious set of expansions that permits the closed form solution of some off-center spherical problems.

The mathematical formulation of the problem is as follows. The electric field, assuming quasi-static conditions, can be expressed as

$$\mathbf{E} = -\nabla V$$

where V is the electrostatic potential. The quasi-static approximation is valid because of the dimensions, frequencies, and electrical properties of the materials involved. In our calculations, the relative complex permittivity (K) of the brain tissue at the typical carrier frequencies used in calcium-ion studies are 100–j175 at 50 MHz, 72–j94.9 at 100 MHz, and 66–j69.2 at 147 MHz [Foster et al, 1979]; for the buffer the values are 71–j580 at 50 MHz, 71–j290 at 100 MHz, and 71–j200 at 147 MHz [Hollis et al, 1980; Stogryn, 1971]. The relative complex permittivity is defined by

$$K = \frac{\sigma + j\omega\epsilon}{j\omega\epsilon_o}$$

The externally applied field, which makes an angle of 90° with the z-axis (i.e., $\mathbf{E} = E_o\hat{\mathbf{u}}_y$) produces a potential that can be expressed in spherical coordinates in the form

$$V_{ext} = -E_o r_a Y^e_{11}(\theta_a,\phi)$$

or

$$V_{ext} = -E_o r_b Y^e_{11}(\theta_b,\phi)$$

where

$$Y^e_{nm}(\theta,\phi) = \cos m\phi\ P^m_n(\cos\theta).$$

The associated Legendre polynomials $P^m_n(\cos\theta)$ are defined as [Morse and Feshbach, 1953]

$$P^m_n(x) = (1 - x^2)^{m/2}\frac{d^m P_n(x)}{dx^m}$$

where $P_n(x)$ are Legendre polynomials.

The potential in regions I, II, and III satisfies Poisson's equation, subject to the appropriate boundary conditions. The charge distributions at $r_a = a$ and $r_b = b$ produce potentials V_a and V_b of the form

$$V_a = \begin{cases} V_{a,in} = \sum_{n=0}^{\infty} \sum_{m=0}^{n} \alpha_{nm} \left(\frac{r_a}{a} \right)^n Y_{nm}^c(\theta_a, \phi) & (r_a \leqslant a) \\ V_{a,out} = \sum_{n=0}^{\infty} \sum_{m=0}^{n} \alpha_{nm} \left(\frac{a}{r_a} \right)^{n+1} Y_{nm}^c(\theta_a, \phi) & (r_a \geqslant a) \end{cases} \tag{1}$$

and

$$V_b = \begin{cases} V_{b,in} = \sum_{n=0}^{\infty} \sum_{m=0}^{n} \beta_{nm} \left(\frac{r_b}{b} \right)^n Y_{nm}^c(\theta_b, \phi) & (r_b \leqslant b) \\ V_{b,out} = \sum_{n=0}^{\infty} \sum_{m=0}^{n} \beta_{nm} \left(\frac{b}{r_b} \right)^{n+1} Y_{nm}^c(\theta_b, \phi) & (r_b \geqslant b) \end{cases} \tag{2}$$

where α_{nm} and β_{nm} are constants to be determined from the boundary conditions. In terms of (1) and (2), the potentials in the three regions are given by

$$V_I = V_{a,in} + V_{b,out} + V_{ext} , \tag{3}$$

$$V_{II} = V_{a,out} + V_{b,out} + V_{ext} , \tag{4}$$

$$V_{III} = V_{a,in} + V_{b,in} + V_{ext} . \tag{5}$$

The form selected for the potentials in (1) and (2) satisfies the continuity conditions at $r_a = a$ and $r_b = b$. Therefore, the boundary conditions that remain to be satisfied at the interface are the continuity of the normal component of the current density at $r_a = a$ and $r_b = b$, namely

$$(\sigma_1 + j\omega\epsilon_1) \frac{\partial V_I}{\partial r_a} \bigg]_{r_a = a} = j\omega\epsilon_0 \frac{\partial V_{II}}{\partial r_a} \bigg]_{r_a = a} \tag{6}$$

and

$$(\sigma_1 + j\omega\epsilon_1) \frac{\partial V_I}{\partial r_b} \bigg]_{r_b = b} = (\sigma_3 + j\omega\epsilon_3) \frac{\partial V_{III}}{\partial r_a} \bigg]_{r_b = b} . \tag{7}$$

In order to apply the boundary conditions at the surface of the off-center sphere (i.e., at $r_b = b$), we need to expand the solution $V_{a,in}$ in terms of the coordinates r_b, θ_b, and ϕ, and the solution $V_{b,out}$ in terms of the coordinates r_a, θ_a, and ϕ. The necessary expansions are [Morse and Feshbach, 1953: 1270–1272]

$$V_{a,in} = \sum_{n=0}^{\infty} \sum_{m=0}^{n} \alpha_{nm} a^{-n} \sum_{s=m}^{n} f_{snm} r_b^s Y_{sm}^e(\theta_b, \phi) \tag{8}$$

and

$$V_{b,out} = \sum_{n=0}^{\infty} \sum_{m=0}^{n} \beta_{nm} b^{n+1} \sum_{s=m}^{n} g_{snm} r_a^{-s-1} Y_{sm}^e(\theta_a, \phi), \tag{9}$$

where

$$f_{snm} = \frac{(-1)^{n-s}(n+m)!d^{n-s}}{(n-s)!(s+m)!}$$

and

$$g_{snm} = \frac{d^{s-n}(s-m)!}{(n-m)!(s-n)!}.$$

Substituting (3), (4), and (5) into (6) and (7), and using (8) and (9), we obtain the following set of linear equations for the $n = p$ ($p = 0,1, \ldots$) and $m = q$ ($q = 0,1, \ldots,n$) coefficients (i.e., α_{pq} and β_{pq}):

$$E_o(1-K_1)\delta_{p,1}\delta_{q,1} + \frac{1}{a}\alpha_{pq}[(p+1) + pK_1] + \sum_{v=q}^{p} \beta_{vq}(1-K_1) \frac{(-1)^{p-v}(p-q)!(p+1)b^{v+1}d^{p-v}}{(v-q)!(p-v)!\, a^{p+2}} = 0 \tag{10}$$

and

$$E_o(1-K_3')\delta_{p,1}\delta_{q,1} + \frac{1}{b}\beta_{pq}[(p+1) + pK_3'] + \sum_{v=p}^{\infty} \alpha_{vq}(K_3'-1) \frac{(-1)^{v-p}(v+q)!pb^{p-1}d^{v-p}}{(v-p)!(p+q)!a^v} = 0, \tag{11}$$

where

$$K_1 = \frac{\sigma_1 + j\omega\epsilon_1}{j\omega\epsilon_o}$$

$$K_3 = \frac{\sigma_3 + j\omega\epsilon_3}{j\omega\epsilon_o}$$

and

$$K_3' = \frac{K_3}{K_1}.$$

In (10) and (11) $\delta_{p,1}$ and $\delta_{q,1}$ are Kronecker deltas.

Fixing the maximum n to be N_{max}, (10) and (11) result in $2N_{max}$ unknowns for each value of m. Various values of the truncation parameter N_{max} were chosen, and it was found that values larger than seven did not alter the solution. Only m=q=1 contributes because the equations are linear and the excitation terms (i.e., the first terms in (10) and (11)) are zero for q=0 or q>1. Using a matrix inversion program (10) and (11) are solved for α_{p1} and β_{p1}, p=0 to N_{max}, and the results are then inserted into (1) to (5) to calculate the potential in the three regions.

The electric field and power density distributions are calculated as follows. The x-component of the electric field is found by numerical differentiation:

$$E_x(x,y,z) = [V(x+\Delta x,y,z) - V(x-\Delta x,y,z)]/2\Delta x,$$

and the same for the other components. The time average absorbed power density is then $\sigma E^2/2$.

RESULTS

The absorbed power density distributions were calculated for a brain volume of 0.3 cm^3, buffer volume of 1 cm^3, and h = 0.05 cm. Therefore, a = 0.677 cm, b = 0.415 cm, d = 0.212 cm, and t = 0.474 cm. Also, the limiting cases as h approaches zero, and d approaches zero are considered. For h → 0 (i.e., when the spheres touch at the bottom) the dimensions are a = 0.677 cm, b = 0.415 cm, d = 0.262 cm, and t = 0.524 cm.

Figures 3 and 4 graphically illustrate the absorbed power density distribution in the (0,y,z) plane produced by an incident carrier wave, with E_o=1 V/m, at 147 MHz for the cases where h = 0.05 cm and d→0, respectively. Each line represents a constant absorbed power density level. The number scale is linear, ranging from zero to nine, where nine represents an absorbed power density of 0.5 mW/m^3. For example, the value of two represents an absorbed power density of (2/9) 0.5 = 0.111 mW/m^3. Also, there are two constant (unlabeled) power density lines between the labeled lines. Each of these lines represents an increment of 1/3. For example, the two lines between 3 and 4, represent 3⅓ and 3⅔. In the brain region of Figure 3, the absorbed power density level varies from a value of 2 toward the top to 2⅓ toward the bottom. In Figure 4 the absorbed power density distribution in the brain region is constant at a value of 0.109 mW/m^3.

The limiting case as h→0 was also calculated, and the values of the absorbed power density used in the calculations of the scaling ratios (see Figs. 5 and 8). The absorbed power density profile was essentially the same as that for the h = 0.05 cm case (see Fig. 3), except the values toward the bottom are somewhat larger.

Similar absorbed power density patterns to the ones shown in Figures 3 and 4 are produced at 50 and 100 MHz, except that the absorbed power levels are smaller.

It is a significant observation from Figure 3 that the absorbed power density distribution in the brain region is not uniform; the bottom of the chick brain has a

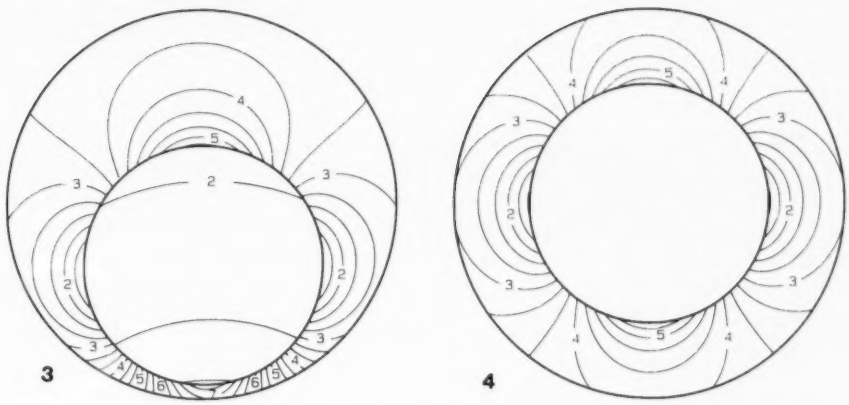

Fig. 3. Absorbed power density distribution at 147 MHz. The dimensions are a = 0.677 cm, b = 0.415 cm, d = 0.212 cm, h = 0.05 cm, and t = 0.474 cm. The number scale (0–9) is linear, where nine represents an absorbed power density of 0.5 mW/m^3 for an incident field of E_o=1 V/m.

Fig. 4. Absorbed power density distribution at 147 MHz for a centered spherical model (d = 0). The dimensions are a = 0.677 cm, b = 0.415 cm, and t =h = 0.262 cm. The number scale (0–9) is linear, where nine represents an absorbed power density of 0.5 mW/m^3 for an incident field of E_o=1 V/m.

higher absorbed power density than the top. On the other hand, Figure 4 shows that the concentric spherical model yields a constant absorbed power density in the brain region. Also, in Figures 3 and 4 the surface fields around the chick brain exhibit a significant variation from the bottom to the top.

SCALING RELATIONS

It has been shown [Joines and Blackman, 1980, 1981] that by maintaining a constant average electric field within the brain tissue, calcium-ion efflux results at one frequency can be used to extrapolate those at another frequency. It is therefore important to be able to determine what incident power densities are required to maintain a constant internal electric field as the frequency of the electromagnetic field changes. The necessary scaling relations can be determined by writing the internal electric field as

$$|\mathbf{E}|^2 = |\mathbf{E}_i|^2 F, \tag{12}$$

where F is related to the electromagnetic absorptive properties of the brain and $\mathbf{E}_i$ is the incident electric field. The incident field is related to the incident power density according to

$$P_i = |\mathbf{E}_i|^2/2\eta_o, \tag{13}$$

where η_o = 377 ohms is the intrinsic impedance of free space. Substituting (13) into (12) and forming the ratio between the internal electric field at two different frequencies yields the following relation

$$\frac{P_i(f_1)}{P_i(f_2)} = \frac{|\mathbf{E}(f_1)|^2}{|\mathbf{E}(f_2)|^2} \cdot \frac{F(f_2)}{F(f_1)},$$

where f denotes the frequency. Requiring a constant internal electric field means that

$$|\mathbf{E}(f_1)| = |\mathbf{E}(f_2)|.$$

Therefore,

$$\frac{P_i(f_1)}{P_i(f_2)} = \frac{F(f_2)}{F(f_1)}. \tag{14}$$

In order to determine values for (14), it is necessary to consider the power absorbed and express it in the form

$$P_a(f) = \frac{1}{2}\sigma|\mathbf{E}_i|^2 F(f).$$

At $f = f_1$, we can determine $P_a(f_1)$ for $E_1 = 1$ V/m then $F(f_1)$ follows. Similarly, at $f = f_2$, we can determine $P_a(f_2)$ and $F(f_2)$ follows. If these values are inserted into (14), the scaling ratios can be determined.

Figures 5 and 6 give the values of the scaling ratios that make the electric field intensity the same at f_1 and f_2 for points along the z-axis inside the spherical brain between the top (i.e., $z = 0.415$ cm) and bottom (i.e., $z = -0.415$ cm). Figures 7 and 8 give values of the scaling ratios that make the electric field intensity the same at f_1 and f_2 for points on the outside surface of the brain between the top (i.e., $\theta = 0$) and the bottom (i.e., $\theta = \pi$) from $0 \leqslant \theta \leqslant \pi$.

Some interesting observations can be made from Figures 5–8. The scaling ratios between two given frequencies are continuous at the top and bottom of the brain–buffer interface. This follows from the fact that electric field is tangential and continuous at the top and bottom brain–buffer interface. For example, at $z = 0.415$ cm in Figure 5 the scaling ratio is identical to the scaling ratio at $\theta = 0$ in Figure 7. The scaling ratio in the concentric spherical case (i.e., when $d = 0$) is constant in the brain region at the value of 3.56 in Figure 5 and 6.57 in Figure 6. The scaling ratio value of 6.57 for $P_i(50)/P_i(147)$ compares favorably with the one obtained by Joines and Blackman [1981], namely 6.6.

DISCUSSION AND CONCLUSIONS

The main objective of this paper was to develop a model of the chick brain/buffer arrangement that was more realistic than previous concentric or isolated spherical models. To that end, an off-center spherical model was used to approximate the physical geometry. This model represents a significant refinement because the brain can be surrounded by unequal amounts of buffer solution on its upper and lower surfaces. The quasi-static formulation of the boundary value problem required the development of zonal harmonic expansions that have not previously appeared in the literature.

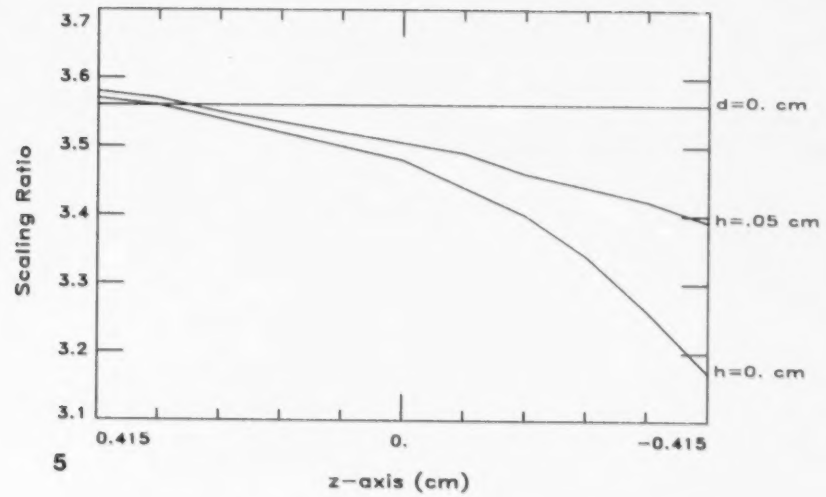

5

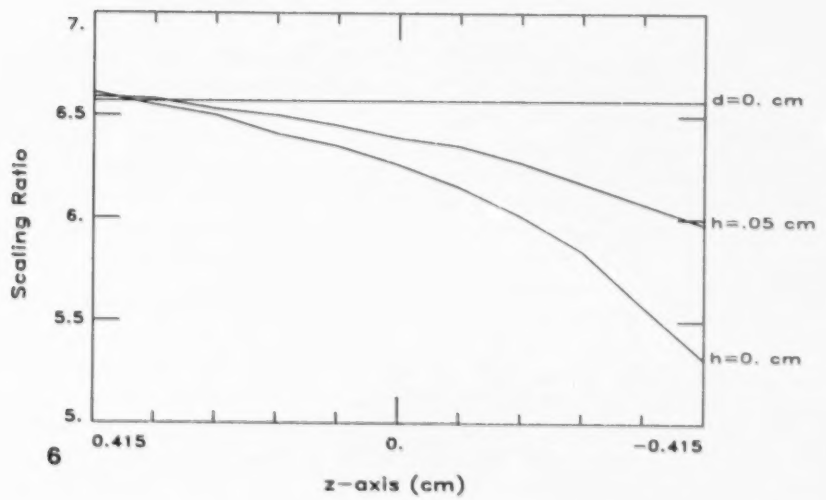

6

Fig. 5. Scaling ratio values for $P_i(50)/P_i(100)$ along the z-axis of the brain.

Fig. 6. Scaling ratio values for $P_i(50)/P_i(147)$ along the z-axis of the brain.

The off-center spherical model revealed that the scaling ratio inside the brain tissue is not constant; the maximum change ($h = 0$ case) from the top of the brain to the bottom was approximately 11% for $P_i(50)/P_i(100)$, and 19% for $P_i(50)/P_i(147)$. This is in contrast to the concentric spherical model that predicts no change. As would be expected, the scaling ratios near the top are essentially identical to the values predicted by the concentric spherical model. At the bottom the values become closer to those predicted by an isolated spherical model. Thus, the off-center spherical

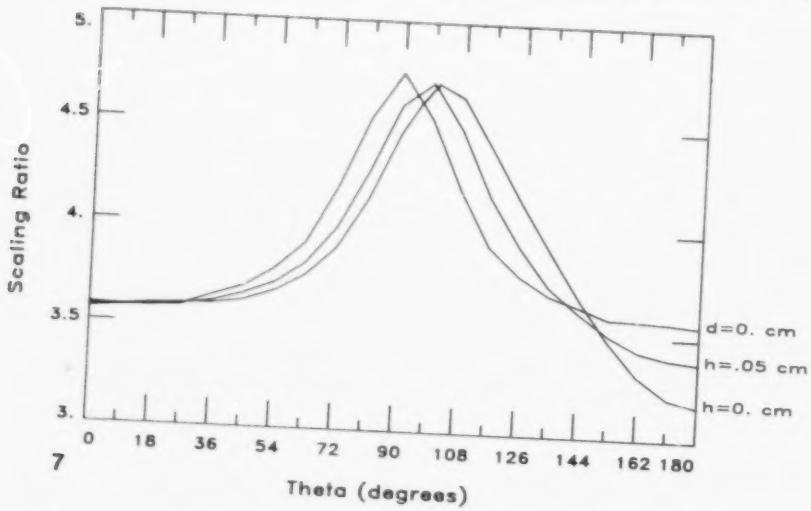

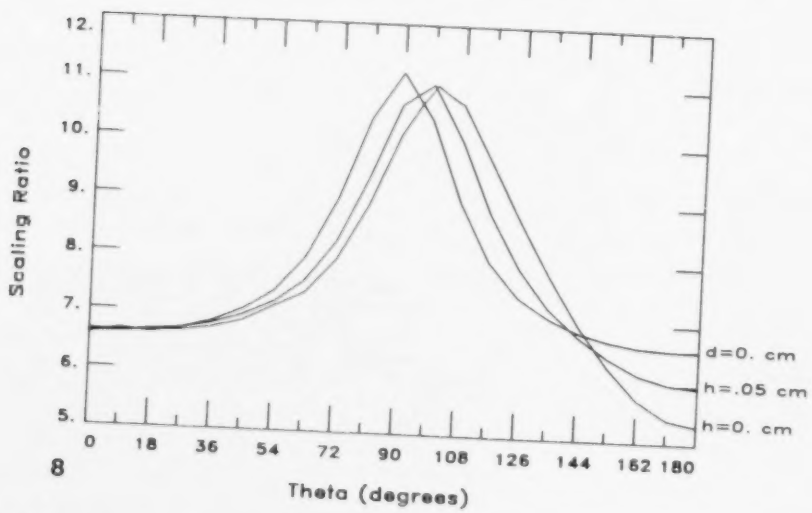

Fig. 7. Scaling ratio values for $P_i(50)/P_i(100)$ along the outside surface of the brain as a function of θ.

Fig. 8. Scaling ratio values for $P_i(50)/P_i(147)$ along the outside surface of the brain as a function of θ.

model yields internal scaling ratios that lie between the extreme values predicted by the concentric and isolated spherical models.

Recent experimental studies [Adey et al, 1982] have shown that the penetration of radioactive calcium ions in chick brain tissue was no greater than 1 mm from the surface. Thus, it may be concluded that surface field values are of paramount importance. To that end, absorbed power density values at the surface of the brain are also shown in Figures 3 and 4, while Figures 7 and 8 plot the related scaling ratios around the surface of the brain. The profiles for the surface scaling ratios are

symmetric for the concentric spherical case, with the peak value occurring at a point on the surface ($\theta = 90°$), where the external electric field is normal to the surface. However, the off-center spherical model yielded somewhat lower peak values whose position shifted toward the bottom ($\theta \approx 99°$). In addition, the surface ratios were similar at the top of the brain for all the models, but the values at the bottom varied considerably, with the h = 0 case approaching the value given for an isolated sphere.

A suggestion for further work is to consider the magnetic field component with an off-center spherical model. The reason for this is that most of the calcium-ion efflux experiments have been conducted with both the electric and magnetic fields present to irradiate the chick brain tissue. While the magnetic field contributes minimally to the absorbed power density ($\approx 3\%$) [Joines and Blackman, 1980] at 147 MHz, and even smaller contributions for frequencies below 147 MHz, it has been reported [Blackman et al, 1984] that the AC–magnetic field component must be present at selected intensities of ELF fields to cause enhanced calcium-ion efflux.

ACKNOWLEDGMENTS

The parts of this research conducted at the University of Miami were supported by the Environmental Protection Agency grant 68-02-4092.

REFERENCES

Adey WR, Bawin SM, Lawrence AF (1982): Effects of weak amplitude-modulated microwave fields on calcium efflux from awake cat cerebral cortex. Bioelectromagnetics 3:295–307.

Bawin SM, Kaczmarck LK, Adey WR (1975): Effects of modulated VHF fields on the central nervous system. Ann NY Acad Sci 247:247–281.

Blackman CF, Elder JA, Weil CM, Benane SG, Eichinger DC, House DE (1979): Induction of calcium-ion efflux from brain tissue by radio-frequency radiation: Effects of modulation frequency and field strength. Radio Sci 14(6S):93–98.

Blackman CF, Benane SG, Elder JA, House DE, Lampe JA, Faulk JM (1980a): Induction of calcium-ion efflux from brain tissue by radio-frequency radiation: Effect of sample number and modulation frequency on the power-density window. Bioelectromagnetics 1:35–43.

Blackman CF, Benane SG, Joines WT, Hollis MA, House DE (1980b): Calcium-ion efflux from brain tissue: Power density vs. internal field intensity dependencies at 50 MHz RF radiation. Bioelectromagnetics 1:277–283.

Blackman CF, Joines WT, Elder JA (1981): Calcium-ion efflux in brain tissue by radiofrequency radiation. In "Biological Effects of Nonionizing Radiation." Illinger, KH (ed): ACS Symposium Series. Washington, DC: American Chemical Society, No. 157, pp. 299–314.

Blackman CF, Benane SG, Rabinowitz JR, House DE, Joines WT (1985): A role for the magnetic component in the field-efflux of calcium-ions from brain tissue in vitro. Bioelectromagnetics 6:327–338.

Blackman CF, Benane SG, House DE, Joines WT (1985): Effects of ELF (1–120 Hz) and modulated (50 Hz) RF fields on the efflux of calcium ions from brain tissue in vitro. Bioelectromagnetics 6:1–11.

Foster KR, Schetps JL, Stoy RD, Schwan HP (1979): Dielectric properties of brain tissue between .01 and 10 GHz. Phys Med Biol 24:1117–1187.

Hollis MA, Blackman CF, Weil CM, Allis JR, Schaefer DJ (1980): A swept-frequency magnitude method for the dielectric characterization of chemical and biological systems. IEEE Trans Microwave Theory Tech MTT-28:791–801.

Joines WT, Blackman CF (1980): Power density field intensity, and carrier frequency determinants of RF-energy-induced calcium-ion efflux from brain tissue. Bioelectromagnetics 1:271–275.

Joines WT, Blackman CF, Hollis MT (1981): Broadening of the RF power-density window for calcium-ion efflux from brain tissue. IEEE Trans Biomed Eng 8:568–573.

Joines WT, Blackman CF (1981): Equalizing the electric field intensity within chick brain immersed in buffer solution at different carrier frequencies. Bioelectromagnetics 2:411–413.
Morse PM, Feshbach H (1953): "Methods of Theoretical Physics." New York: McGraw-Hill.
Sheppard AR, Bawin SM, Adey WR (1979): Models of long-range order in cerebral macromolecules: Effects of sub-ELF and modulated VHF and UHF fields. Radio Sci. 14:141–145.
Stogryn A (1971): Equation for calculating the dielectric constant of a saline water. IEEE Trans Microwave Theory Tech MTT-19:733–736.
Weil CM, Spiegel RC, Joines WT (1984): Internal field strength measurements in chick forebrains at 50, 147, and 450 MHz. Bioelectromagnetics 5:293–304.

NOTICE

This document has been reviewed in accordance with U.S. Environmental Protection Agency policy and approved for publication. Mention of trade names or commercial products does not constitute endorsement or recommendation for use.

This article documents research that was conducted under the auspices of the U.S. Environmental Protection Agency (USEPA). As an arm of the government, the USEPA has a paid up, non-exclusive, irrevocable, worldwide license to reproduce, prepare derivative works, and distribute to the public all of the material contained herein, and to grant others acting on its behalf the right to do so. The USEPA grants to the National Technical Information Service, Department of Commerce, the right to act as its agent in the distribution of this material.